Supplementary Material:

Towards a lumped approach for solid plastic waste gasification: polyethylene and polypropylene pyrolysis

• • •

Andrea Locaspi, Matteo Pelucchi, Marco Mehl, Tiziano Faravelli

CRECK Modeling Lab, Department of Chemistry Materials and Chemical Engineering, Politecnico di Milano, Milan, Italy

S1. Species Definition

As described in Section 2.1 of the main text, the present model introduces several lumped and real species to describe the polymer pyrolysis. The functional groups introduced to describe high molecular weight species (HMW) are schematically represented in Table S1 for both polymers.

Table S1
HMW species introduced in the kinetic Mechanism

Species	Polyethylene		Polypropylene	
	Name	Representation	Name	Representation
MC stable paraffin	P-C21H42-P(L)	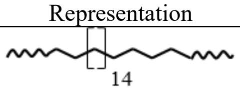	P-IC21H42-P(L)	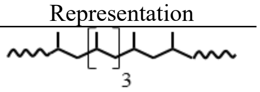
EC stable paraffin	P-C21H43(L)	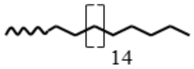	P-IC21H43t(L)	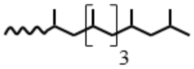
			P-IC21H43h(L)	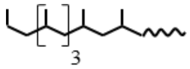
EC stable olefin	P-C21H41(L)	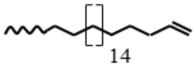	P-IC21H41t(L)	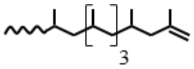
			P-IC21H41h(L)	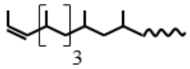
MC radical	P-C21H41-P(L)	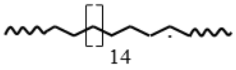	P-IC21H41-P(L)	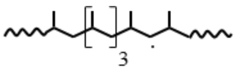
EC paraffin internal radical	P-C21H42(L)	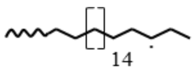	P-IC21H42t(L)	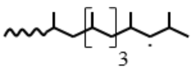
			P-IC21H42h(L)	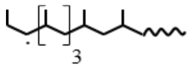
EC paraffin	P-C21H42_T(L)		P-IC21H42t_T(L)	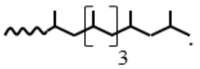

terminal radical		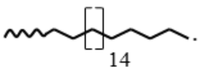	P-IC21H42h_T(L)	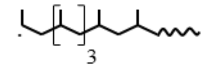
EC olefin internal radical	P-C21H42(L)	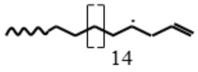	P-IC21H42t(L)	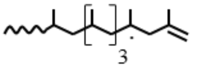
			P-IC21H42h(L)	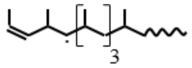
EC olefin allyl-type radical	P-C21H42_A(L)	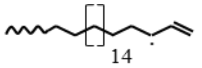	P-IC21H42t_A(L)	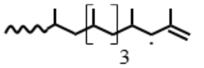
			P-IC21H42h_A(L)	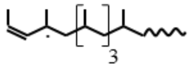

The species considered in the present mechanism are functional groups of N_C=21 as HMW, C_1-C_{10} as RLMW and C_{15}, C_{21}, C_{30}, C_{39} as LLMW for a total of 74 species for PE. For PP the same HMW and RLMW are employed while the LLMW introduced due to the head and tail configurations are C_{17}, C_{18}, C_{19}, C_{26}, C_{27}, C_{28}, C_{35}, C_{36}, and C_{37} resulting in 126 species. The choice of the considered species affects the model predictions both in terms of mass loss profiles and product distribution. The division of species in RLMW and LLMW also affects computational costs as introducing LLMW species also increases the number of radicals. Fig. S1 shows the comparison of model predictions in terms of mass loss and product distribution varying the considered species for HDPE at HR=5°C/min. The 1st model has been described in the main text, while the others differ by the range of distribution lumped as LLMW species and the number of LLMW species employed (Section 2.1). The 2nd model simplifies the product distribution neglecting reactivity for N_C<12 and evaporation for N_C>36, resulting in 70 species, while the 3rd and 4th model account for an increased range of reactivity although further reducing the number of species (54 and 42 respectively). The 5th and 6th models involve the highest number of liquid-phase species (162 and 172 respectively) but describe with high accuracy the reactivity of LLMW products.

The mass loss profile (Fig. S1a) is affected if evaporation of long chains is not considered. For instance, the 4th and 5th models predict a mass loss profiles shifted at higher temperatures by ~10°C as they do not consider evaporation of chains in the range C_{30}-C_{39}. Considering evaporation of C_{30}-C_{36} as the 2nd and 3rd models shifts the mass loss profiles closer to the presented model (C_{10}-C_{42}, 4 LLMW). The mass loss profiles of the 3rd model are slightly delayed compared to the 2nd model because it does not properly account for evaporation of small species in the C_6-C_{36} range as it introduces only 2 LLMW. Similarly, the 4th model does not properly account for the reactivity and evaporation at N_C>C_6.

Considering the product distribution (Fig. S1b-d), all models similarly describe the chain distribution within a ~20% error margin except for the 3rd and 4th model which significantly underestimate C_6 formation due to the simplified description of LLMW and their backbiting reactions. The 5th and 6th models are the ones describing the impact of backbiting reactions with the highest accuracy, as they account also for decomposition of the formed short chains, but at a significantly higher computational cost. The models with a sharp decrease in predicted distribution (i.e., 4th and 5th) are the same ones predicting a mass loss profiles shifted at higher temperatures.

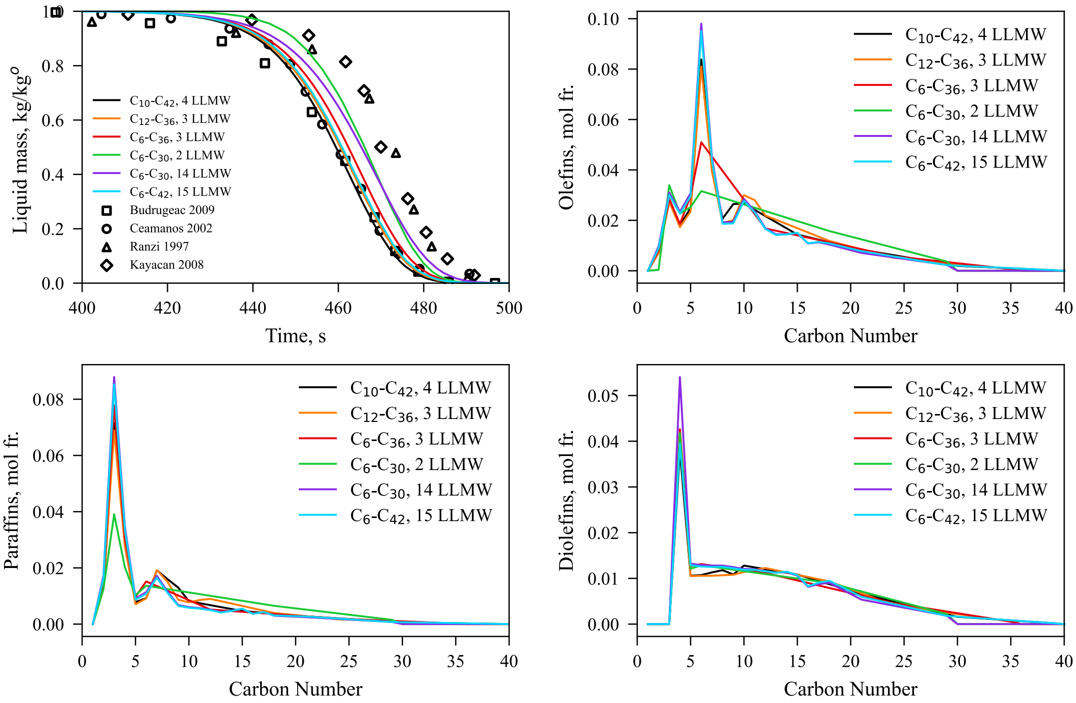

Fig. S1. HDPE pyrolysis at HR=5°C/min, predictions of the present model considering a different number of reactive lumped light molecular weight species (LLMW) to describe different parts of the distribution. The first carbon number in the model label represents the maximum RLMW, while the second number represents the minimum HMW. Comparison for: a) predicted mass loss profiles (lines) with experimental data (Budrugeac, 2010; Ceamanos et al., 2002; Kayacan and Doğan, 2008; Ranzi et al., 1997) (marks), b) final olefins gas molar fractions, c) final paraffins gas molar fractions, d) final diolefins gas molar fractions.

S2. Model Validation

With respect to Section 4 of the main text, additional validation targets from literature are reported in the present section. The model performances are compared with the ones from Faravelli et al. (1999) and experimental data employing the Curve Matching (CM) Score as quantification (Pelucchi et al., 2019). Because of the different x-scales, physical interpretations, and way data are reported, CM scores from dynamic and isothermal runs cannot be compared in an absolute value. Indeed, while for dynamic experiment a CM<0.9 is unsatisfactory, in isothermal runs CM>0.85 represents good agreement. Fig. S2 shows the comparison of mass loss profile for HDPE and LDPE at different operating conditions. For non-isothermal conditions (Fig. S2a-c), the lumped model predictions agree with both the model of Faravelli et al. (1999) and experimental data with an error <10°C in terms of temperature. The only exception are experiments at heating rate (HR) 50°C/min and experiments of Kumar and Singh (2011) which exhibit significantly different behaviors that neither model can predict. The proposed model underestimates the onset temperature at low pressure by ~20°C (Fig. S2c) which is possibly due to overestimation of bubble pressure (Section 3 and 5 of the main text). In general, for dynamic conditions the models have similar Curve Matching scores representing comparable quality in model predictions. Considering isothermal conditions (Fig. S2d-f), the lumped model is in line with the model of Faravelli et al. (1999) but predicts a higher apparent activation energy compared to experimental data.

Indeed, at low temperatures the models predict a lower reactivity compared to experimental data, while the predicted reactivity is higher at higher temperatures. With respect to Fig. S2f, neither model is able to describe the measured mass-loss profiles, as highlighted by the null CM score. Indeed, the authors measure considerable formation of char which is in contrast with other studies (Dogu et al., 2021; Faravelli et al., 1999; Poutsma, 2003) and not accounted for by the models, which may explain the lower reactivity at high conversions. Fig. S2g-h show model predictions for LDPE at 10^{-5} mmHg and different isothermal conditions. As with Fig. S2c, the proposed model is not able to properly describe evaporation, possibly due to evaporation of chains with $N_C>42$ or high bubble pressures. Nevertheless, increasing temperature (Fig. S2h), the agreement of model predictions with experimental data improves considerably. The differences between samples at the same nominal temperature is due both to different molecular weights and different real operating temperatures reported by Jellinek et al. (1949). As discussed in Section 5 of the main text, the proposed model has a low sensitivity to the initial average molecular weight as the model from Faravelli et al. (1999), while experimental data have a slightly stronger effect. In general, both models predict a higher effect of temperature than initial molecular weight while experimental data measure similar reactivities as observed considering the differences between the 412°C 23k MW and 400°C 16k MW (blue and green lines in Fig. S2h),

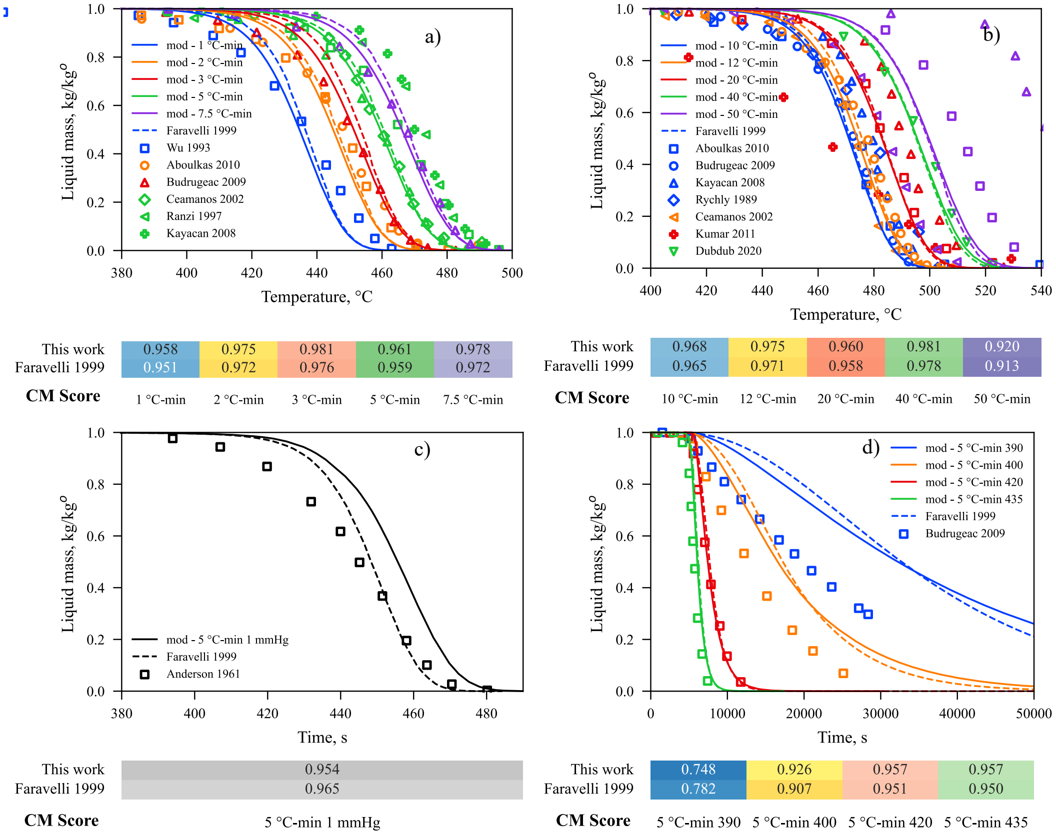

This work	0.958	0.975	0.981	0.961	0.978
Faravelli 1999	0.951	0.972	0.976	0.959	0.972
CM Score	1 °C-min	2 °C-min	3 °C-min	5 °C-min	7.5 °C-min

This work	0.968	0.975	0.960	0.981	0.920
Faravelli 1999	0.965	0.971	0.958	0.978	0.913
CM Score	10 °C-min	12 °C-min	20 °C-min	40 °C-min	50 °C-min

This work	0.954
Faravelli 1999	0.965
CM Score	5 °C-min 1 mmHg

This work	0.748	0.926	0.957	0.957
Faravelli 1999	0.782	0.907	0.951	0.950
CM Score	5 °C-min 390	5 °C-min 400	5 °C-min 420	5 °C-min 435

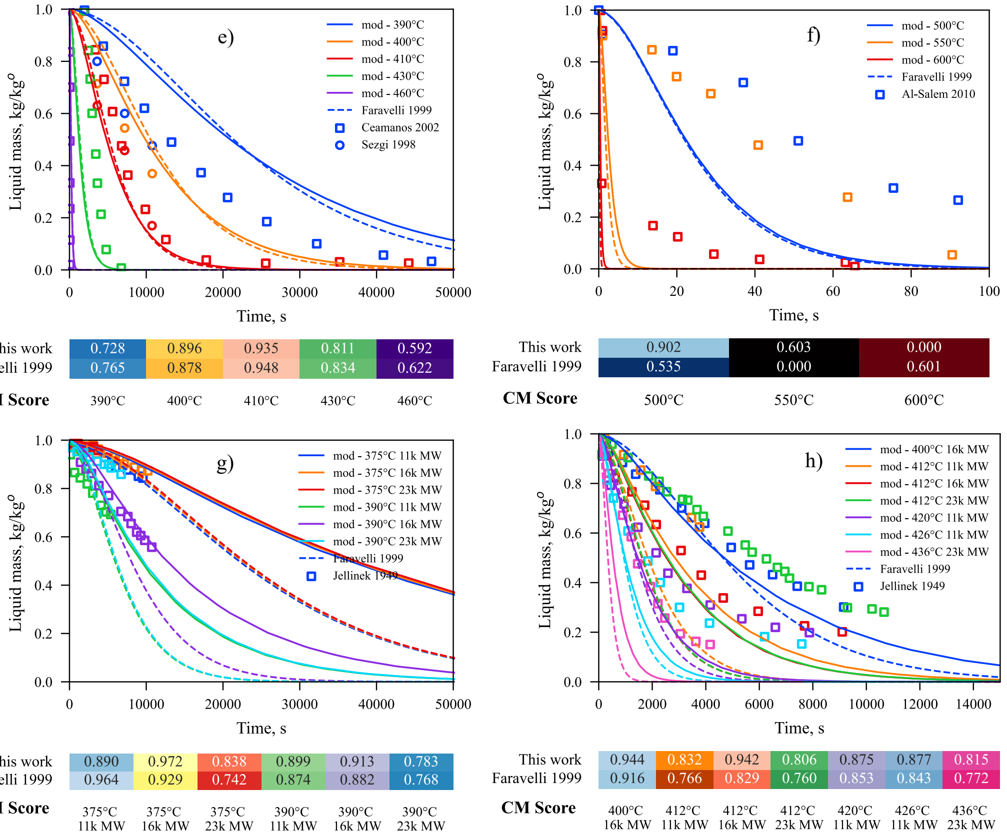

This work	0.728	0.896	0.935	0.811	0.592
Faravelli 1999	0.765	0.878	0.948	0.834	0.622
CM Score	390°C	400°C	410°C	430°C	460°C

This work	0.902	0.603	0.000
Faravelli 1999	0.535	0.000	0.601
CM Score	500°C	550°C	600°C

This work	0.890	0.972	0.838	0.899	0.913	0.783
Faravelli 1999	0.964	0.929	0.742	0.874	0.882	0.768
CM Score	375°C 11k MW	375°C 16k MW	375°C 23k MW	390°C 11k MW	390°C 16k MW	390°C 23k MW

This work	0.944	0.832	0.942	0.806	0.875	0.877	0.815
Faravelli 1999	0.916	0.766	0.829	0.760	0.853	0.843	0.772
CM Score	400°C 16k MW	412°C 11k MW	412°C 16k MW	412°C 23k MW	420°C 11k MW	426°C 11k MW	436°C 23k MW

Fig. S2. Mass loss profiles of PE at various operating conditions for: a-f) HDPE, g,h) LDPE. Comparison of the present model (solid lines), the model from (Faravelli et al., 1999) (dashed lines), and experimental data (symbols) from (Aboulkas et al., 2010; Al-Salem and Lettieri, 2010; Anderson and Freeman, 1961; Budrugeac, 2010; Ceamanos et al., 2002; Jellinek, 1949; Kayacan and Doğan, 2008; Khaghanikavkani et al., 2011; Kumar and Singh, 2011; Ranzi et al., 1997; Rychlý and Rychlá, 1989; Sezgi et al., 1998)

Fig. S3 shows the predicted mass loss profiles for PP at different operating conditions. Considering dynamic conditions (Fig. S3a-d), the present model predicts a higher apparent activation energy with respect to experimental data, but lower than the detailed model of Faravelli et al. (1999) because of the different kinetic constants employed. Indeed, while it overestimates the experimental onset temperature by ~10°C, it underpredicts the final experimental decomposition temperature by ~5°C. With respect to isothermal conditions (Fig. S3e-f), the models predict different apparent activation energies and different reactivities. Indeed, as highlighted by the CM score, according to the experimental conditions one model appears better than the other, but overall they exhibit similar behaviours. Fig. S3f shows the comparison between APP and IPP in terms of both model predictions and experimental data. For both APP and IPP the model underestimates the experimental low temperature reactivity. Nevertheless, the model agrees with experimental data of Fig. S3e which are in the same temperature range of Fig. S3f. The model requires also further validation at non-atmospheric pressure conditions.

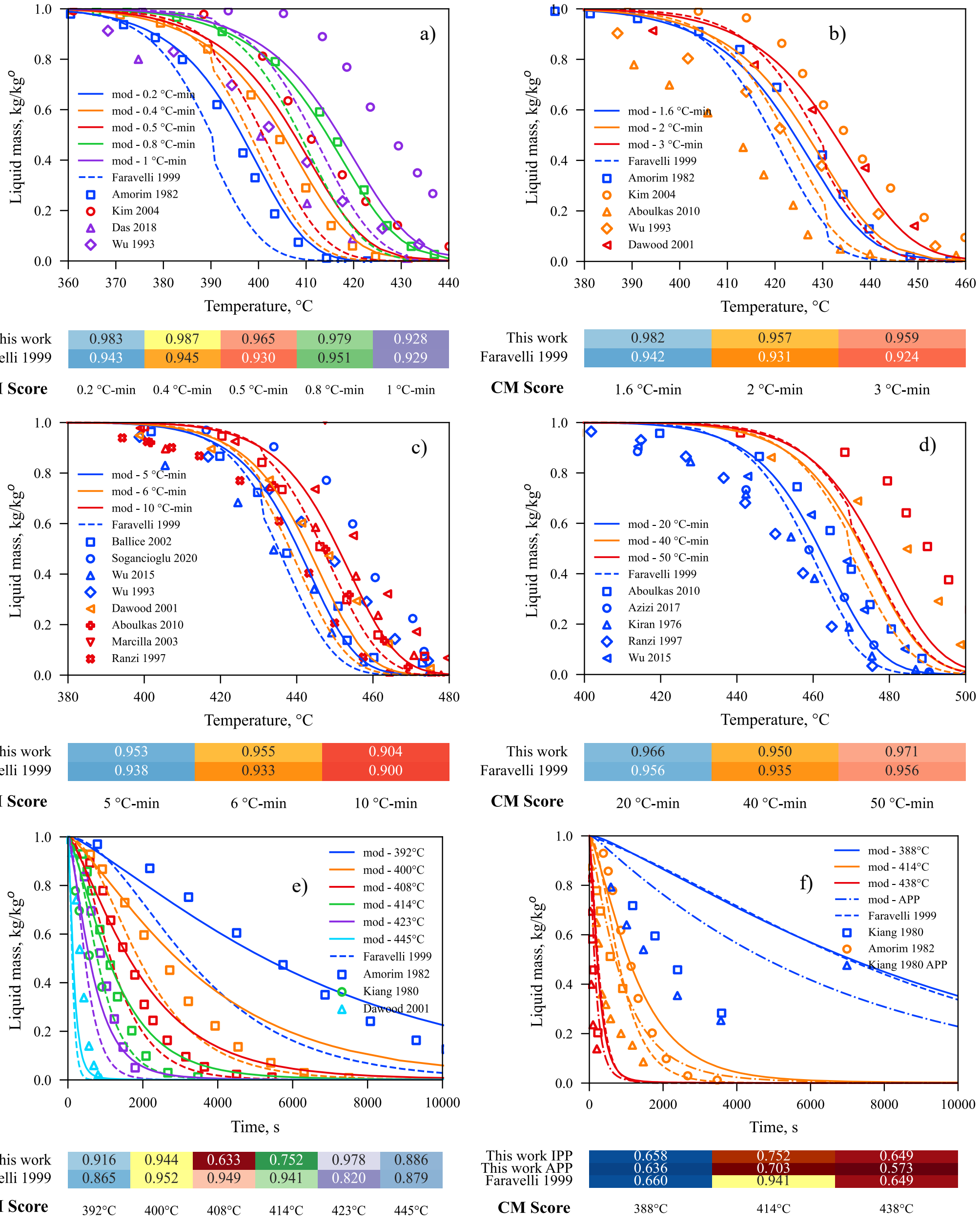

CM Score	0.2 °C-min	0.4 °C-min	0.5 °C-min	0.8 °C-min	1 °C-min
This work	0.983	0.987	0.965	0.979	0.928
Faravelli 1999	0.943	0.945	0.930	0.951	0.929

CM Score	1.6 °C-min	2 °C-min	3 °C-min
This work	0.982	0.957	0.959
Faravelli 1999	0.942	0.931	0.924

CM Score	5 °C-min	6 °C-min	10 °C-min
This work	0.953	0.955	0.904
Faravelli 1999	0.938	0.933	0.900

CM Score	20 °C-min	40 °C-min	50 °C-min
This work	0.966	0.950	0.971
Faravelli 1999	0.956	0.935	0.956

CM Score	392°C	400°C	408°C	414°C	423°C	445°C
This work	0.916	0.944	0.633	0.752	0.978	0.886
Faravelli 1999	0.865	0.952	0.949	0.941	0.820	0.879

CM Score	388°C	414°C	438°C
This work IPP	0.658	0.752	0.649
This work APP	0.636	0.703	0.573
Faravelli 1999	0.660	0.941	0.649

Fig. S3. Mass loss profiles of PP at various operating conditions for: a-d) IPP, e) APP and IPP. Comparison of the present model (solid lines), the model from (Faravelli et al., 1999) (dashed lines), and experimental data (symbols) from (Aboulkas et al., 2010, 2007; Azizi et al., 2017; Ballice and Reimert, 2002; Das and Tiwari, 2018; Dawood and Miura, 2001; Kiang et al., 1980; Kim and Kim, 2004; Kiran and Gillham, 1976; Marcilla et al., 2003; Ranzi et al., 1997; Rychlý and Rychlá, 1989; Sogancioglu et al., 2020; Sousa Pessoa De Amorim et al., 1982; Wu et al., 2015)

The model has been also assessed with experimental data on product distribution. However, as discussed in Section 2.2. of the main text, the model inevitably predicts a paraffin, olefin, diolefin molar ratio of 0.25:0.5:0.25 satisfying the hydrogen balance. On the other hand, experimental results predict equimolar amounts of paraffins, and olefins as discussed by

Poutsma (2003). Fig. S4 show the comparison of the gaseous products normalized molar fraction for PP and PE at different operating conditions. The model correctly describes the spiked product distribution of PP, except for experimental data of Kim and Kim (2004) (Fig. S4a-c) which exhibit different peaks. The model predicts preferential release of C_9 and C_6 hydrocarbons due to 1-5 backbiting reactions consistently with the other experimental data, while C_8 forms from 1-4 backbiting which however is favored only at temperatures >700°C. Considering experiments of Kiang et al. (1980) (Fig. S4d-f), the simplified approach introduced to model tacticity does not introduce any product selectivity for APP and IPP. The model shows good agreement with predictions of the model and experimental data of Kruse et al. (2003) (Fig. S4g-l) for both paraffins and olefins distribution, although it underestimates C_8 paraffin, possibly due to the high selectivity towards C_5 paraffin. As mentioned in Section 4 of the main text, the authors also report data on dialkenes which the present model significantly overpredicts and are not reported in the present work. Furthermore, while the model correctly describes the product selectivity, compared to the model of Kruse et al. (2003) it overestimates mass loss profiles as it also predicts the release of species with a higher carbon number. Fig. S4m-n shows comparison of model predictions with experimental data on paraffin formation at high temperatures for PE. As with APP, the model does not introduce any selectivity towards branched or linear products from PE pyrolysis but is nevertheless able to describe the total carbon distribution (Fig. S4m). Considering the effect at increasing temperatures (Fig. S4n), the model predicts similar distributions for the three cases, although the model predicts that unzipping, leading to C_2 formation, becomes dominant at 920 °C. The model does not describe the experimental increase in C_3 formation since it forms from allyl reactions which are favored at low temperatures.

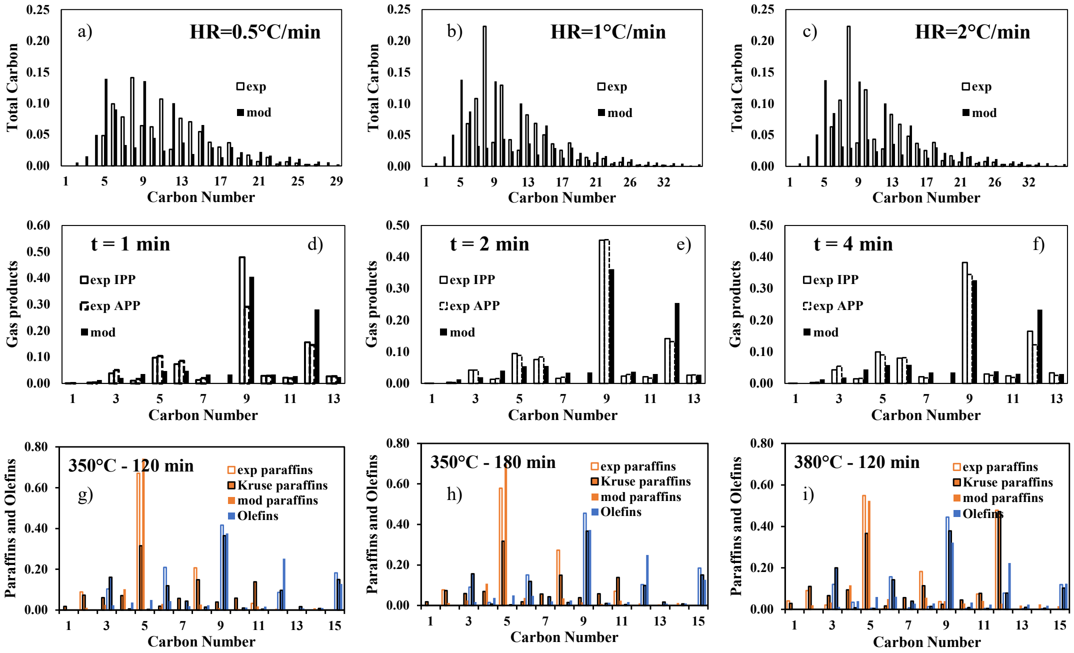

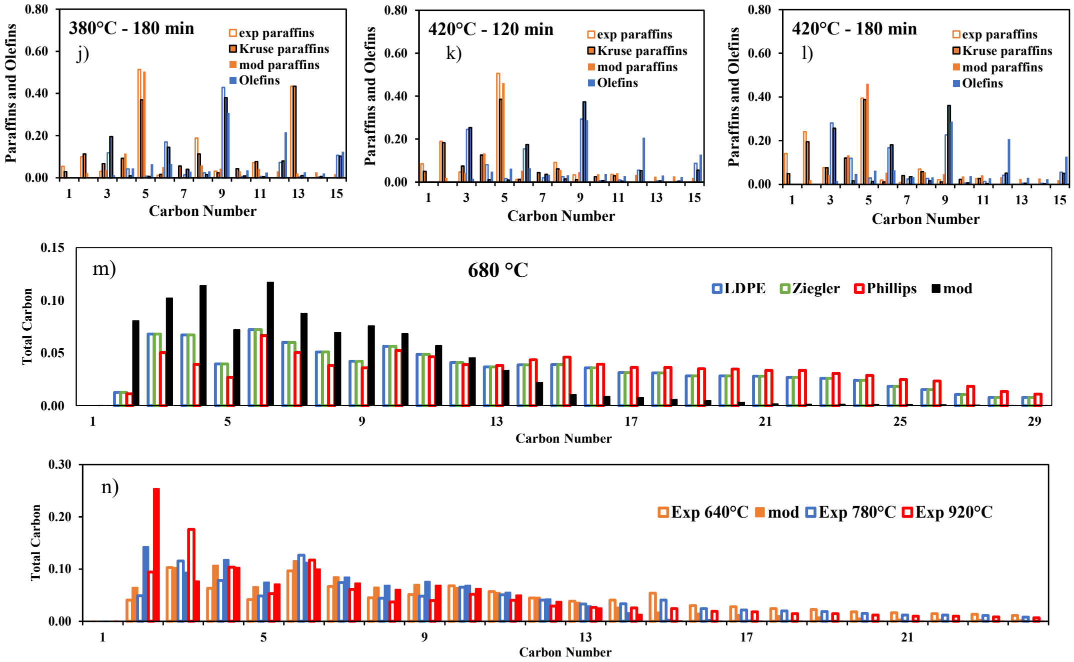

Fig. S4. Gas mole fractions normalized on the shown products for: a-l) IPP and APP, m,n) HDPE and LDPE. Comparison of the present model (solid lines), the model of Kruse et al. (Kruse et al., 2003) (dashed lines), and experimental data (symbols) from (Kiang et al., 1980; Kim and Kim, 2004; Kruse et al., 2003; Michajlov et al., 1968)

References

Aboulkas, A., El harfi, K., El Bouadili, A., 2010. Thermal degradation behaviors of polyethylene and polypropylene. Part I: Pyrolysis kinetics and mechanisms. Energy Convers. Manag. 51, 1363–1369. https://doi.org/10.1016/j.enconman.2009.12.017

Aboulkas, A., El Harfi, K., El Bouadili, A., Ben Chanâa, M., Mokhlisse, A., 2007. Pyrolysis kinetics of polypropylene. J. Therm. Anal. Calorim. 2007 891 89, 203–209. https://doi.org/10.1007/S10973-007-7398-Z

Al-Salem, S.M., Lettieri, P., 2010. Kinetic study of high density polyethylene (HDPE) pyrolysis. Chem. Eng. Res. Des. 88, 1599–1606. https://doi.org/10.1016/J.CHERD.2010.03.012

Anderson, D.A., Freeman, E.S., 1961. The kinetics of the thermal degradation of polystyrene and polyethylene. J. Polym. Sci. 54, 253–260. https://doi.org/10.1002/POL.1961.1205415920

Azizi, K., Keshavarz Moraveji, M., Abedini Najafabadi, H., 2017. Characteristics and kinetics study of simultaneous pyrolysis of microalgae Chlorella vulgaris, wood and polypropylene through TGA. Bioresour. Technol. 243, 481–491. https://doi.org/10.1016/J.BIORTECH.2017.06.155

Ballice, L., Reimert, R., 2002. Classification of volatile products from the temperature-programmed pyrolysis of polypropylene (PP), atactic-polypropylene (APP) and thermogravimetrically derived kinetics of pyrolysis. Chem. Eng. Process. Process Intensif. 41, 289–296. https://doi.org/10.1016/S0255-2701(01)00144-1

Budrugeac, P., 2010. Theory and practice in the thermoanalytical kinetics of complex processes: Application for the isothermal and non-isothermal thermal degradation of HDPE. Thermochim. Acta 500, 30–37. https://doi.org/10.1016/J.TCA.2009.12.007

Ceamanos, J., Mastral, J.F., Millera, A., Aldea, M.E., 2002. Kinetics of pyrolysis of high density polyethylene. Comparison of isothermal and dynamic experiments. J. Anal. Appl. Pyrolysis 65, 93–110.

https://doi.org/10.1016/S0165-2370(01)00183-8

Das, P., Tiwari, P., 2018. The effect of slow pyrolysis on the conversion of packaging waste plastics (PE and PP) into fuel. Waste Manag. 79, 615–624. https://doi.org/10.1016/j.wasman.2018.08.021

Dawood, A., Miura, K., 2001. Pyrolysis kinetics of γ-irradiated polypropylene. Polym. Degrad. Stab. 73, 347–354. https://doi.org/10.1016/S0141-3910(01)00096-9

Dogu, O., Pelucchi, M., Van de Vijver, R., Van Steenberge, P.H.M., D'hooge, D.R., Cuoci, A., Mehl, M., Frassoldati, A., Faravelli, T., Van Geem, K.M., 2021. The chemistry of chemical recycling of solid plastic waste via pyrolysis and gasification: State-of-the-art, challenges, and future directions. Prog. Energy Combust. Sci. 84, 100901. https://doi.org/10.1016/j.pecs.2020.100901

Faravelli, T., Bozzano, G., Scassa, C., Perego, M., Fabini, S., Ranzi, E., Dente, M., 1999. Gas product distribution from polyethylene pyrolysis. J. Anal. Appl. Pyrolysis 52, 87–103. https://doi.org/10.1016/S0165-2370(99)00032-7

Jellinek, H.H.G., 1949. Thermal degradation of polystyrene and polyethylene. Part III. J. Polym. Sci. 4, 13–36. https://doi.org/10.1002/POL.1949.120040102

Kayacan, I., Doğan, Ö.M., 2008. Pyrolysis of low and high density polyethylene. Part I: Non-isothermal pyrolysis kinetics. Energy Sources, Part A Recover. Util. Environ. Eff. 30, 385–391. https://doi.org/10.1080/15567030701457079

Khaghanikavkani, E., Mohammed, ;, Farid, M., 2011. Thermal Pyrolysis of Polyethylene: Kinetic Study. Energy Sci. Technol. 2, 1–10. https://doi.org/10.3968/j.est.1923847920110201.597

Kiang, J.K.Y., Uden, P.C., Chien, J.C.W., 1980. Polymer reactions-Part VII: Thermal pyrolysis of polypropylene. Polym. Degrad. Stab. 2, 113–127. https://doi.org/10.1016/0141-3910(80)90033-6

Kim, S.S., Kim, S.S., 2004. Pyrolysis characteristics of polystyrene and polypropylene in a stirred batch reactor. Chem. Eng. J. 98, 53–60. https://doi.org/10.1016/S1385-8947(03)00184-0

Kiran, E., Gillham, J.K., 1976. Pyrolysis-molecular weight chromatography: A new on-line system for analysis of polymers. II. Thermal decomposition of polyolefins: Polyethylene, polypropylene, polyisobutylene. J. Appl. Polym. Sci. 20, 2045–2068. https://doi.org/10.1002/APP.1976.070200803

Kruse, T.M., Wong, H.W., Broadbelt, L.J., 2003. Mechanistic Modeling of Polymer Pyrolysis: Polypropylene. Macromolecules 36, 9594–9607. https://doi.org/10.1021/MA030322Y

Kumar, S., Singh, R.K., 2011. Recovery of hydrocarbon liquid from waste high density polyethylene by thermal pyrolysis. Brazilian J. Chem. Eng. 28, 659–667. https://doi.org/10.1590/S0104-66322011000400011

Marcilla, A., Gómez, A., Reyes-Labarta, J.A., Giner, A., 2003. Catalytic pyrolysis of polypropylene using MCM-41: Kinetic model. Polym. Degrad. Stab. 80, 233–240. https://doi.org/10.1016/S0141-3910(02)00403-2

Michajlov, L., Zugenmaier, P., Cantow, H.J., 1968. Structural investigations on polyethylenes and ethylene-propylene copolymers by reaction gas chromatography and X-ray diffraction. Polymer (Guildf). 9, 325–343. https://doi.org/10.1016/0032-3861(68)90042-6

Pelucchi, M., Stagni, A., Faravelli, T., 2019. Addressing the complexity of combustion kinetics: Data management and automatic model validation. Comput. Aided Chem. Eng. 45, 763–798. https://doi.org/10.1016/B978-0-444-64087-1.00015-2

Poutsma, M.L., 2003. Reexamination of the Pyrolysis of Polyethylene: Data Needs, Free-Radical Mechanistic Considerations, and Thermochemical Kinetic Simulation of Initial Product-Forming Pathways. Macromolecules 36, 8931–8957. https://doi.org/10.1021/ma0303768

Ranzi, E., Dente, M., Faravelli, T., Bozzano, G., Fabini, S., Nava, R., Cozzani, V., Tognotti, L., 1997. Kinetic modeling of polyethylene and polypropylene thermal degradation. J. Anal. Appl. Pyrolysis 40–41, 305–319. https://doi.org/10.1016/S0165-2370(97)00032-6

Rychlý, J., Rychlá, L., 1989. Non-isothermal thermogravimetry of polymer - I. General model involving formal termination of active centres. J. Therm. Anal. 35, 77–90. https://doi.org/10.1007/BF01914266

Sezgi, N.A., Cha, W.S., Smith, J.M., McCoy, B.J., 1998. Polyethylene Pyrolysis: Theory and Experiments for Molecular-Weight-Distribution Kinetics. Ind. \& Eng. Chem. Res. 37, 2582–2591. https://doi.org/10.1021/ie980106r

Sogancioglu, M., Yel, E., Ahmetli, G., 2020. Behaviour of waste polypropylene pyrolysis char-based epoxy composite materials. Environ. Sci. Pollut. Res. 27, 3871–3884. https://doi.org/10.1007/S11356-019-07028-3/TABLES/9

Sousa Pessoa De Amorim, M.T., Bouster, C., Veron, J., 1982. Pyrolysis of polypropylene. II. Kinetics of degradation. J. Anal. Appl. Pyrolysis 4, 103–115. https://doi.org/10.1016/0165-2370(82)80002-8

Wu, X., Wu, Y., Wu, K., Chen, Y., Hu, H., Yang, M., 2015. Study on pyrolytic kinetics and behavior: The co-pyrolysis of microalgae and polypropylene. Bioresour. Technol. 192, 522–528. https://doi.org/10.1016/j.biortech.2015.06.029